The Arabidopsis COBRA protein facilitates cellulose crystallization at the plasma membrane

Nadav Sorek, Hagit Sorek, Aleksandra Kijac, Heidi J. Szemenyei, Stephan Bauer, Kian Hematy, David E. Wemmer, Chris R. Somerville

THE JOURNAL OF BIOLOGICAL CHEMISTRY VOL. 289, NO. 50, pp. 34911–34920, December 12, 2014

The *Arabidopsis* COBRA Protein Facilitates Cellulose Crystallization at the Plasma Membrane*

Received for publication, August 26, 2014, and in revised form, October 14, 2014 Published, JBC Papers in Press, October 20, 2014, DOI 10.1074/jbc.M114.607192

Nadav Sorek[‡§1], Hagit Sorek[‡], Aleksandra Kijac[¶], Heidi J. Szemenyei[‡§], Stefan Bauer[‡], Kian Hématy[‖], David E. Wemmer[‡¶], and Chris R. Somerville[‡§‡‡]**

*From the [‡]Energy Biosciences Institute, the [§]Plant and Microbial Biology Department, and the [¶]Department of Chemistry, University of California, Berkeley, California 94720, the [‖]INRA, Institut Jean-Pierre Bourgin, UMR 1318, ERL CNRS3559, Saclay Plant Sciences, RD10, F-78026 Versailles, France, **AgroParisTech, Institut Jean-Pierre Bourgin, UMR 1318, ERL CNRS3559, Saclay Plant Sciences, RD10, F-78026 Versailles, France, and [‡‡]Department of Arid Land Agriculture, Faculty of Meteorology, Environment and Arid Land Agriculture, King Abdulaziz University, 21589 Jeddah, Saudi Arabia*

Background: The *COBRA* gene is highly coexpressed with cellulose synthase genes, but its function remains unclear.
Results: COBRA localizes at the plasma membrane and binds glucan chains. NMR studies indicate structural defects in cellulose in the mutant despite normal polymerization rate.
Conclusion: COBRA functions downstream of cellulose biosynthesis.
Significance: This work suggests that alignment of glucan chains into cellulose fibrils is fa[illegible]d by one or more proteins.

Mutations in the *Arabidopsis COBRA* gene lead to defects in cellulose synthesis but the function of COBRA is unknown. Here we present evidence that COBRA localizes to discrete particles in the plasma membrane and is sensitive to inhibitors of cellu[illegible] lose synthesis, suggesting that COBRA and the cellulos[illegible] thase complex reside in close proximity on the pla[illegible] brane. Live-cell imaging of cellulose synthesis[illegible] once initiated, cellulose synthesis appeare[illegible] in the *cobra* mutant. Using isotherma[illegible] found to bind individual β1–4-li[illegible] 3.2 μM. Competition assay[illegible] ual β1–4-linked glucan[illegible] line cellulose. Solid-state[illegible] the cell wall of the *cobra* m[illegible]on to decreases in cellulose amo[illegible]ellulose fibrils and other cell wall poly[illegible] wild type by being less crystalline and having[illegible] number of reducing ends. We interpret the availab[illegible]ence as suggesting that COBRA facilitates cellulose crystallization from the emerging β1–4-glucan chains by acting as a "polysaccharide chaperone."

Cellulose microfibrils comprise the core component of the cell walls that surround each plant cell, allowing a mode of growth based on turgor pressure (1). In higher plants, cellulose is synthesized at the plasma membrane by the cellulose synthase complex (2, 3), which is comprised of multiple cellulose synthase proteins (CESA),[2] although their exact stoichiometry is unknow[illegible] CESA proteins synthesize β1–4[illegible] with each other, and by [illegible]fibril (3). Cellulose synmembrane has been connection to cortical [illegible]has been demonstrated (2, 6). individual glucan chains form celains elusive. Because it is challenging to plant cellulose synthesis *in vitro*, genetic been used to identify and characterize the genes [illegible]eins that participate in cellulose synthesis and deposi[illegible] (7). *KORRIGAN* was one of the earliest genes that was implicated in cellulose synthesis (8). KORRIGAN was shown to act as an endo-1,4-β-glucanase (9), and it was also shown to have multiple effects on the composition of the cell wall (10, 11). Although the function of KORRIGAN is known and an interaction with the cellulose synthase complex has been shown (12, 13), the role of KORRIGAN in cellulose formation is still unclear.

Co-expression analysis helped to identify several other genes required for different aspects of cellulose formation (14). Like *CSI1* and *KORRIGAN*, chitinase-like genes are co-expressed with the CESAs and were shown to be involved in cellulose formation (15). Chitinase-like proteins were suggested to play a key role in establishing interactions between cellulose microfibrils and hemicelluloses, which are thought to coat the cellulose microfibrils.

COBRA is one of the genes that is most highly co-expressed with the primary CESA family (14). The *Arabidopsis COBRA* gene was originally identified in a screen for root defects (16). In *Arabidopsis*, the *COBRA* family contains 11 members with different expression patterns. Of these genes, *COBRA* has the highest and most widely distributed expression (17).

Mutations in *COBRA* cause dramatic reduction in cellulose levels (18). Inspection of the orientation of cellulose fibrils in cobra mutants by electron microscopy suggested that the orientation of the cellulose fibrils was affected (19). COBRA was

* This work was supported in part by grants from the Energy Biosciences Institute (to C. R. S. and D. E. W.).
[1] Recipient of Postdoctoral Award FI-434-2010 from the Binational Agricultural Research and Development Fund. To whom correspondence should be addressed: Energy Biosciences Institute, University of California Berkeley, 1521 Berkeley Way, Berkeley, CA 94704. Tel.: 510-643-6265; E-mail: nadavsorek@berkeley.edu.
[2] The abbreviations used are: CESA, cellulose synthase proteins; GPI, glycophosphatidylinositol; CBM, cellulose binding motif; ssNMR, solid-state NMR; MAS, magic angle spinning.

shown to be glycophosphatidylinositol (GPI) anchored, as well as *N*-glycosylated (19). GPI-anchored proteins are typically targeted to the outer leaflet of the plasma membrane (20). Based on phase separation, COBRA was detected in both endomembranes as well as in the plasma membrane fraction, whereas immunolabeling demonstrated localization at the Golgi and the cell wall, but not at the plasma membrane (19). However, immunolabeling of the rice ortholog showed that COBRA localized mainly at the plasma membrane in young, developing tissue, and primarily in the cell wall in mature tissue (21). Therefore, it was suggested that its localization is dependent on tissue type and developmental stage.

The *COBRA* sequence harbors a putative cellulose binding motif (CBM) (22), and the rice COBRA CBM was shown to bind cellulose (21). COBRA was tested against a variety of cell wall polymers, and was found to bind specifically to cellulose. However, the binding was significantly higher when tested against a crude cellulose fraction compared with Avicel, a purified cellulose powder (21).

In this work, we succeeded in using live imaging to visualize COBRA and establish its presence in distinct particles at the plasma membrane. By using isothermal titration calorimetry we showed that COBRA can bind individual β1–4-glucan chains with an dissociation constant (K_D) of 3.2 ± 0.1 μM. Furthermore, COBRA binding to individual β1–4-gluc competes with its binding to pure cellulose observations suggest that COBRA acts at t lulose biosynthesis, when emerging form cellulose fibrils. Using soli nance (ssNMR) we chara mutant in detail, demo lose crystallization.

EXPERIMENTAL PROCEDURES

Molecular Cloning

All plasmids are listed in Table 1. Oligonucleotides are listed in Table 2. Gateway cloning was performed according to the manufacturer's instructions (Invitrogen). *COBRA* was subcloned into pGEX4T-2 with oligonucleotide primers NS173 and NS174 to create GST-His$_6$-COBRA (pNS87). The *COBRA* CDS (lacking the signal peptide and GPI motif sequence) with the sequence CATCATCCAGGCCATCAT (encodes the FlAsH tag, -Cys-Cys-Pro-Gly-Cys-Cys) inserted after tyrosine 37 (FlAsH-COBRA) was synthesized by DNA2.0. FlAsH-*COBRA* was amplified using oligonucleotides NS29 and NS30 and cloned into pDONOR207 to create plasmid NS38. 2.5 kb of the *COBRA* promoter was amplified using oligonucleotides NS31 and NS33 and cloned into pDONOR P4-P1R to create plasmid NS29. Plasmids NS29, NS38, and NS60 were used to create the expression vector p*COBRA*::FlAsH-*COBRA*:NOS in pH7 mu34GW (plasmid N by multigateway reaction.

Plant Growth C

Arabid eeds and various mutant line rminated on Murashige th MS salts, 0.8% agar, own vertically on the for 5 days before being hamber at 22 °C under a 16-h

opy

SA6 imaging—For analyses of YFP-CESA6 pro- seeds were germinated on MS agar plates and grown ertically in darkness for 5 days at 22 °C. Seedlings were mounted between two coverslips in water. Imaging was performed on a Yokogawa CSUX1 spinning-disk system featuring the DMI6000 Leica motorized microscope and a Leica ×100/1.4 numerical aperture oil objective. YFP was excited at 488 nm, and a band-pass filter (510/20 nm) was used for emission filter-

TABLE 1
Plasmids used in this study

Plasmid name	Descri	Source
pGEX4T-2	N terminus GST expression	GE Healthcare
PCR8	Entry vector	Invitrogen
pDONOR P4-P1R	Promoter entry vector	psb.ugent.be
pDONOR 207	1st gene entry vector	psb.ugent.be
pDONOR P2R-P3	2nd gene entry vector	psb.ugent.be
pH7 mu34GW	Plant expression vector	psb.ugent.be
NS29	*COBRA* 2.5-kb promoter in pDONOR P4-P1R	This study
NS38	FlAsH-COBRA in pDONOR207	This study
NS60	NOS terminator in pDONOR P2R-P3	41
NS79	pCOB::FlAsh-COBRA:NOS in pH7 mu34GW	This study
NS85	His$_6$-COBRA in PCR8	This study
NS87	GST-His6-COBRA in pGEX4T-2	This study

TABLE 3
Transgenic plant lines used in this study

Transgenic line	Genotype	Source
cob-6	*cobra*	SALK_051906
YFP:CESA6	pCESA6::YFP:CESA6, prc$^{-/-}$	24
GFP:CESA3	pCESA3::GFP:CESA3, eli1–1$^{-/-}$	42
YFP:CESA6 x *cob-6*	pCESA6::YFP:CESA6, prc$^{-/-}$; cob-6$^{-/-}$	This study
FlAsH-COBRA line1	pCOBRA::FlAsH-COBRA, cob-6$^{-/-}$	This study
FlAsH-COBRA line2	pCOBRA::FlAsH-COBRA, cob-6$^{-/-}$	This study
FlAsH-COBRA line3	pCOBRA::FlAsH-COBRA, cob-6$^{-/-}$	This study

TABLE 2
Primers used in this study

Primer name	Sequence (5′ to 3′)	Product of target
NS29	GGGGACAAGTTTGTACAAAAAAGCAGGCT ATGGAGTCTT TCTTC	5′ FlAsH-COBRA into p207
NS30	GGGGACCACTTTGTACAAGAAAGCTGGGT TTAGGCAGAGAAGAAGAA	3′ FlAsH-COBRA into p207
NS31	GGGGACAACTTTGTATAGAAAAGTTG GATCTTGATGATGAATGGAA	5′ *COBRA* promoter into pDONOR P4-P1R
NS33	GGGGACTGCTTTTTTGTACAAACTTG TTTTAATACTCTGATGATC	3′ *COBRA* promoter into pDONOR P4-P1R
NS173	CTCGAGAACATCATCATCATCATCACTTTACTTCGACAGAAGCATA	5′ His$_6$:COBRA CDS, no SP and no GPI seq
NS174	GCTCGAGTCAGGGAAGAAAAGGGTA	3′ *COBRA* CDS, no SP and no GPI seq
NS180	TTTGTGCTCCAACCATACTCC	*COBRA* LP
NS181	AAGCAAAGCACCTTCCTCTTC	*COBRA* RP
Lbb1	ATTTTGCCGATTTCGGAAC	cob-6 LP

ing. Image analysis was performed using Metamorph (Molecular Devices) and Imaris (Bitplane) software.

Movies were collected at 5 days from randomly selected seedlings of the various genotypes. Movies were taken at ambient temperatures. An approximately equal number of acquisitions were attempted for each, with poor focal quality movies discarded during post-processing (data not shown).

Image analysis was performed with ImageJ and Imaris software. Movies were first contrast enhanced in ImageJ, and a walking average of four frames was taken using the kymograph plug-in for ImageJ. These steps were performed to improve the accuracy of automated particle recognition performed in subsequent steps. These images were opened in Imaris 6.2.1 and switched from Z-series to time series. The pixel size was set to 135 nm/pixel based on measurements from the microscope, and the time interval was set to 5 s. The particle-recognition algorithm in Imaris was performed with a spot size of 250 nm. High-intensity signal was filtered to eliminate Golgi signal. Following this, the connected components program was run, which determines particle identity over several frames and converts the movement of the particle into tracks. All tracks present for less than 60 s (12 frames) were discarded. The displacement and duration of the remaining tracks were exported to a spreadsheet, and their average velocity was calculated.

FlAsH-COBRA Imaging—FlAsH labeling was do… reported previously (23). Seeds of FlAsH-COBRA w… sterilized in 2.4% sodium hypochlorite with 0.1… four times in water, and suspended in 0.1… dark for at least 2 days before planti… on vertical 0.8% agar plates co… and Skoog salts (Caisson L… Murashige and Skoog m… m^{-2} s^{-1} light at 21 °C fo… the plate and placed in 1.5-… ing 2 μM Lumio green (Invitrog… m liquid 0.5× Murashige and Skoog m… for 60 min in the dark with gentle shaking. T… were washed twice with Disperse Blue 3 (Invitrogen) … mounted on slides for observation as described in the YFP-CESA6 imaging section.

Isoxaben Treatments—Isoxaben treatments were carried out as previously reported (24). GFP-CESA3 and FlAsH-COBRA seeds were surface sterilized and plated as described in the GFP-CESA3 imaging section. Seedlings were treated for 30 min with 100 nM Isoxaben.

Plasmolysis—FlAsH-COBRA seedlings were plasmolyzed by incubation in 0.8 M NaCl for 10 min. Seedlings were mounted on microscope slides in the plasmolysis solution.

Protein Expression and Purification

Escherichia coli DH5α was used for DNA propagation. For protein expression, pNS87 was transformed into *E. coli* BL21 CodonPlus DE3 RIL (Stratagene) cells. Cells were grown to A_{600} of 0.6. Protein expression was induced by adding 2 mM isopropyl β-D-thiogalactopyranoside. Protein extraction and purification was carried out with AKTA-prime (GE Healthcare, UK) using HisTRAP FF and GSTrap HP columns according to the manufacturer's instructions (GE Healthcare, UK).

Protein Immunoblots—Anti-His_6 antibodies (Sigma, H1029) were used at a dilution of 1:3,000 together with blotting grade horseradish peroxidase-conjugated goat anti-rabbit immunoglobulin G (Bio-Rad). Detection was performed with SuperSignal West Pico Chemiluminescent Substrate (Pierce, catalog number 15168).

Isothermal Titration Calorimetry

Isothermal titration calorimetry experiments were performed in NanoITC^{2G} (TA Instruments) (25). Measurements were made at 21 °C. The proteins were dialyzed extensively against 50 mM Tris-Cl buffer, pH 7.5, and the cellohexaose was dissolved in the same buffer to minimize heats of dilution. Titrations were carried out in triplicate, and the errors are the mean ± S.D. of these replicates. During a titration experiment the 50 μM protein sample stirred at 250 rpm in a 1.43-ml reaction cell was injected with 15 successive 15-μl aliquots of 750 μM cellohexaose at 300-s intervals. Integrated heat effects, after correction for heats of dilu…n, were analyzed by Sigmaploid dose-response + Hill sl… maPlot). The fitted data yielded the dissociation c… mber of binding sites on the protein (n), … ding (ΔH).

COB… petition Assay

…26. Proteins were incu… (1 mg/ml) in 20 mM … NaCl for 120 min. Avicel … as washed 3 times with 20 mM … 150 mM NaCl. Avicel-bound proteins … ting in SDS sample buffer for 5 min at … ected to SDS-PAGE.

…l Analysis

Seedlings grown vertically on plates were placed in the dark for 24 h to reduce starch levels before harvesting. The alcohol-insoluble residues fraction was prepared by grinding 150 mg of seedling tissue in liquid nitrogen, followed by one extraction with 1 ml of 70% ethanol and three extractions with 1 ml of chloroform:methanol (1:1, v/v). The pellet was washed in 1 ml of acetone and dried overnight under vacuum. Cellulose analysis was based on a modified version of Saeman hydrolysis according to Bauer and Ibáñez (27). In brief, cellulose content was determined by subtracting hemicellulosic glucose released by hydrolysis with 4% sulfuric acid from total glucose released by a two-stage acid hydrolysis. From each sample, two 1-mg aliquots of alcohol-insoluble residue were prepared. The first was treated with 50 μl of 72% sulfuric acid (room temperature, 1 h) to disrupt the cellulose crystalline structure; sulfuric acid was then diluted to 4% by adding 1.4 ml of H_2O and the mixture was heated (121 °C, 60 min). The second aliquot was treated with 1.45 ml of 4% sulfuric acid shortly before heating (121 °C, 60 min). After cooling at room temperature, the reaction mixture was vortexed, and a 1:50 dilution was used for HPLC analysis.

Released monosaccharides were analyzed using an ICS-3000 HPLC system (Thermo Fisher Scientific) equipped with a pulse-amperometric detector. Samples were injected onto a 150 × 3-mm CarboPac PA20 column (Thermo Fisher Scientific) with a 50 × 3-mm guard column of the same material and eluted at 30 °C with 2 mM potassium hydroxide at a flow rate of

0.4 ml/min. Cellulose content (mg of cellulose/mg of dry tissue) was calculated by subtracting the amount of glucose released by 4% sulfuric acid hydrolysis from the amount of glucose released by 72% sulfuric acid treatment. For neutral sugar and uronic acid analysis, a 1-mg aliquot of alcohol-insoluble residue was hydrolyzed with 1.45 ml of 4% sulfuric acid and the mixture was heated (121 °C, 60 min). Samples were cooled and vortexed, and a 1:50 dilution was used for HPLC analysis as above. For uronic acids, samples were injected onto a 250 × 3-mm CarboPac PA200 column with a 30 × 3-mm guard column and eluted at 30 °C using a 50 to 200 mM sodium acetate gradient (in 0.1 M NaOH) at 0.4 ml/min.

Cell Wall Structural Analysis by ^{13}C-MAS ssNMR

All ^{13}C-ssNMR spectra were acquired on a 17.6 T (700 MHz ^{1}H frequency) Bruker Avance spectrometer equipped with a 3.2-mm E_{free} triple resonance magic angle spinning (MAS) probe from Bruker. The spectra were recorded at a 14 kHz magic angle spinning (MAS) rate and a temperature of 280 K. ^{13}C-Labeled chemical shifts were referenced externally to adamantane signal at 38.48 ppm (28).

^{13}C direct polarization experiments with a long recycle delay, 20 s, were used for quantitative measurements. Spectra were acquired with a 48-ms acquisition time, 83 kHz ^{1}H SPINAL-64 decoupling (29), and a 5-μs pulse width on ^{13}C. ^{13}C-Lab chemical shifts were assigned based on reported assignments (30).

Two-dimensional ^{13}C-^{13}C chemical shift relation spectra were acquired with rotational resonance mixing time at 273 K, 14 kHZ spinning f tion parameters were ^{1}H SPINAL-64 decoup Rows X 9.5 us) with States time (5120 × 9.4 μs), and were processed with 0.28 ppm (50 ng (Lorentzian-to-Gaussian apodization) to 8192 (F2) × 2048 (F1) complex points before transformation. These experiments were performed to obtain through-space correlations and to observe changes in the cell wall structure.

RESULTS

To visualize COBRA in live tissue, we created two transgenic lines expressing YFP-COBRA under the native promoter. In the first line, YFP was inserted after Pro^{42}, five amino acids after the predicted secretion peptide cleavage site. In the second line, the YFP tag was inserted before the GPIω site, at Pro^{427}. In both lines we used 2.5 kb upstream of the ATG as a promoter sequence. However, these constructs did not complement the phenotype of the mutant in the 10 independent lines examined, implying the fusion protein was non-functional.

Thus, to visualize COBRA in live tissue we used FlAsH labeling, which involves the modification of the COBRA protein by the addition of a small peptide motif that binds derivatives of fluorescein (23). The tetracysteine motif (Cys-Cys-Pro-Gly-Cys-Cys) was placed immediately after the predicted secretion peptide cleavage motif at Tyr^{37}. The FlAsH-COBRA construct expressed under the control of the native *COBRA* promoter complemented the *cob-6* phenotype, implying functionality of FlAsH-COBRA. Due to low penetration of the FlAsH dyes into hypocotyl cells, FlAsH-COBRA imaging was done in elongating root cells in 5-day-old light grown seedlings (Fig. 1). FlAsH-COBRA was found to localize mainly at the plasma membrane in a punctate pattern (Fig. 1*A*). Plasma membrane localization of FlAsH-COBRA was further confirmed by plasmolysis (Fig. 1*B*). Unfortunately, the FlAsH tag bleached rapidly during laser illumination so we were not able to obtain useful measurements of FlAsH-COBRA movement. However, we observed movement of the particles, although they appeared to move more slowly than the GFP-CESA particles and were significantly less abundant (Fig. 1*A*).

To further investigate the association between COBRA and the cellulose synthase complex, seedlings expressing FlAsH-COBRA were treated with the cellulose synthase complex inhibitor, isoxaben (32). Isoxaben is thought to specifically act on the cellulose synthase co plex because point mutations in CESA3 confer resistan drug (33). Treatment of seedlings with 100 nM min caused almost complete depletion of complex from the plasma membr different focal planes, we us fluorescence as a refer- m) was referred to as was referred to as the , *lower scheme*). Isoxaben sing FlAsH-COBRA showed a e signal from the plasma membrane COBRA could be detected only within the The similar effect of isoxaben on both GFP- FlAsH-COBRA puncta suggests a relationship en the two proteins. One possibility is that the presence of OBRA on the plasma membrane is dependent upon the presence of the CESA complex.

The effect of the *cob-6* mutation on cellulose synthesis was visualized by live-cell imaging of cellulose synthase complexes labeled with YFP (Fig. 1*D*). The average velocity of the cellulose synthase complex in 5-day-old seedlings was 225 nm/min in WT and 289 nm/min in *cob-6* (Fig. 1*E*). The average apparent lifetime of the CESA6-YFP-labeled complex in the *cob-6* background, measured as "tracks" in time-averaged images, was shorter, but the directionality of the tracks was unaffected and linear movement was maintained (Fig. 1*D*). Thus, the basis for the cellulose deficiency was not apparent from direct observation of cellulose synthesis. These sets of data suggest that COBRA acts at the plasma membrane, adjacent to the cellulose synthase complex. Therefore, we tested whether COBRA could interact with the product of the cellulose synthase complex, β1–4-linked glucan (Fig. 2).

COBRA contains a putative CBM (19), and it was recently shown that the purified CBM region from *Brittle Culm1*, a COBRA-like protein from rice, can bind cellulose (21). The fact that *COBRA* contains a GPI anchor (19) implies that this association occurs on the plasma membrane outer leaflet. Therefore, we tested if COBRA could interact with individual β1–4-glucan chains. We expressed COBRA from *Arabidopsis* in *E. coli* without the secretion peptide and the GPI motifs that are cleaved during protein maturation. Binding, affinity, and stoichi-

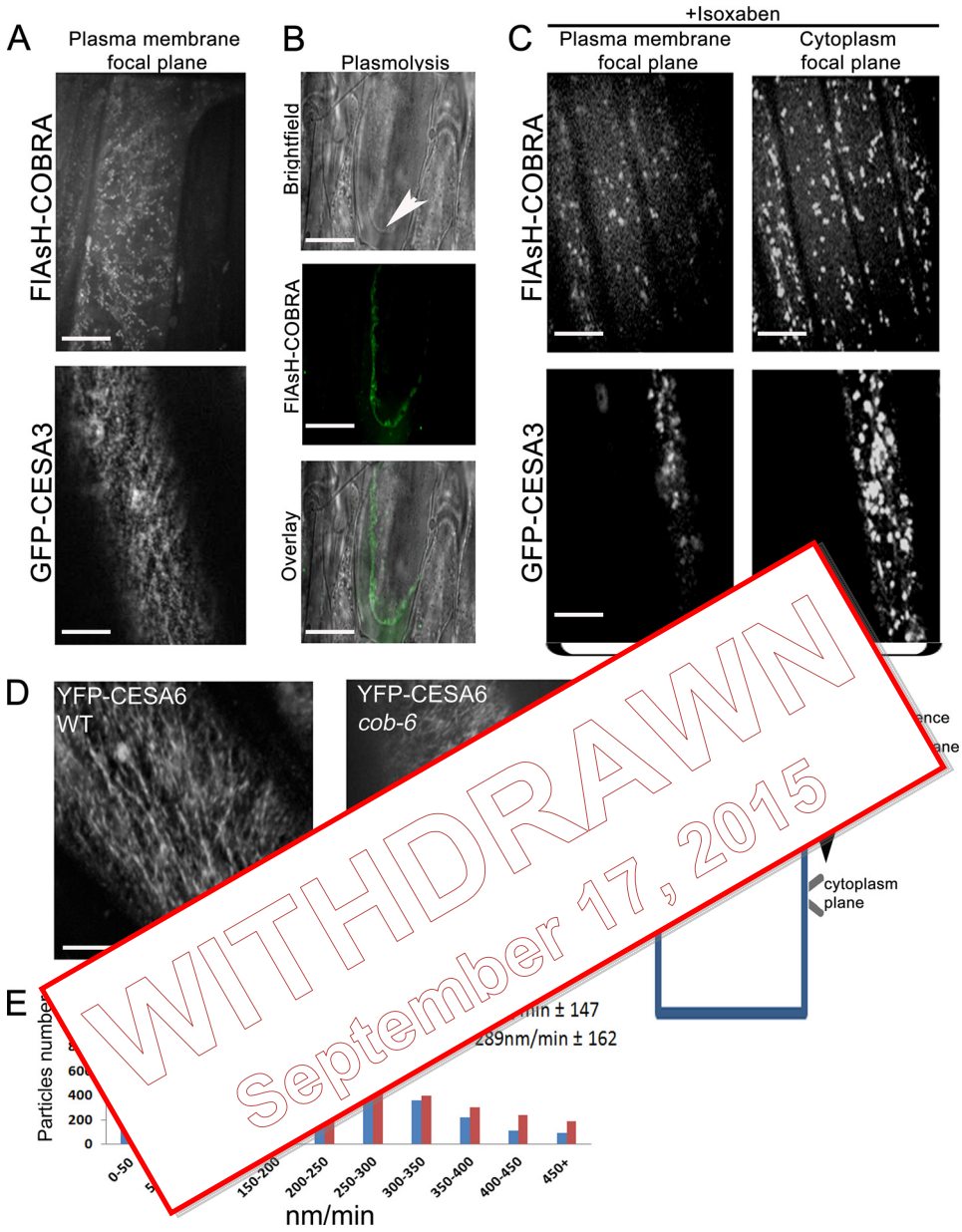

FIGURE 1. **COBRA is localized at the plasma membrane, is sensitive to isoxaben, and when mutated disrupts cellulose synthesis.** *A,* FlAsH-COBRA and GFP-CESA3 were visualized in the hypocotyl elongation zone of 5-day-old dark grown *Arabidopsis* seedlings. FlAsH-COBRA showed a punctate pattern of labeling in the plasma membrane focal plane. *B,* plasma membrane localization was verified by plasmolysis with 0.8 M NaCl, which causes shrinkage and condensation of the cytoplasm and vacuole, and detachment of the plasma membrane from the cell wall (*arrowhead*). *C,* treatment of seedlings with 100 nM isoxaben caused clearance of GFP-CESA3 particles from the plasma membrane resulting in intracellular accumulation. The same observation was made for FlAsH-COBRA treated with isoxaben. *D,* time-lapse confocal images of YFP-CESA6 in hypocotyl cells of 5-day-old etiolated Col-0 (*left*) and *cob-6* (*right*) plants were compared. Each image is an average of 36 frames taken at 5-s intervals ($n = 9$). CESA complex velocities were measured using Imaris. Data passed normality and equal distribution tests after natural log transformation. The complex velocity in *cob-6* (289 ± 162 nm/min) was found to be significantly different from that of wild type (225 ± 147 nm/min) (*t* test, $p < 0.01$). Aside from the differences in the velocity rate, in *cob-6*, cellulose synthesis occurs in a relatively linear direction. Scale bars are 5 μm in *A*, *B*, and *D* and 10 μM in *C*.

ometry of COBRA for cellohexaose was determined by isothermal titration calorimetry (Fig. 2). From these results, the number of ligand molecules bound to COBRA (n), the dissociation constant (K_D), and the binding enthalpy (ΔH) were evaluated. Monomeric carbohydrate-binding proteins generally have a 1:1 ratio with their oligosaccharide ligands (34). Similarly, COBRA was also found to bind one molecule of cellohexaose per protein molecule ($n = 0.94 \pm 0.02$). The enthalpy of binding, ΔH, is negative with a value of -8.2 ± 0.4 kcal mol^{-1} (Fig. 2) implying that the reaction is exothermic. The binding association constant of COBRA to cellohexaose was found to be 3.2 ± 0.1 μM, which is similar to other proteins containing CBMs (35).

Because COBRA was shown to bind cellulose (21), we tested the affinity to crystalline cellulose *versus* the affinity to individual glucan chains (Fig. 3). Avicel is a 95% pure crystalline cellulose with an average particle size of 50 μm. Because Avicel is not soluble, competition assays with cellohexaose were carried out using pulldown assays (26). COBRA was incubated for 2 h at 21 °C with Avicel in the presence of increasing concentrations of cellohexaose. The samples were analyzed using an anti-His_6

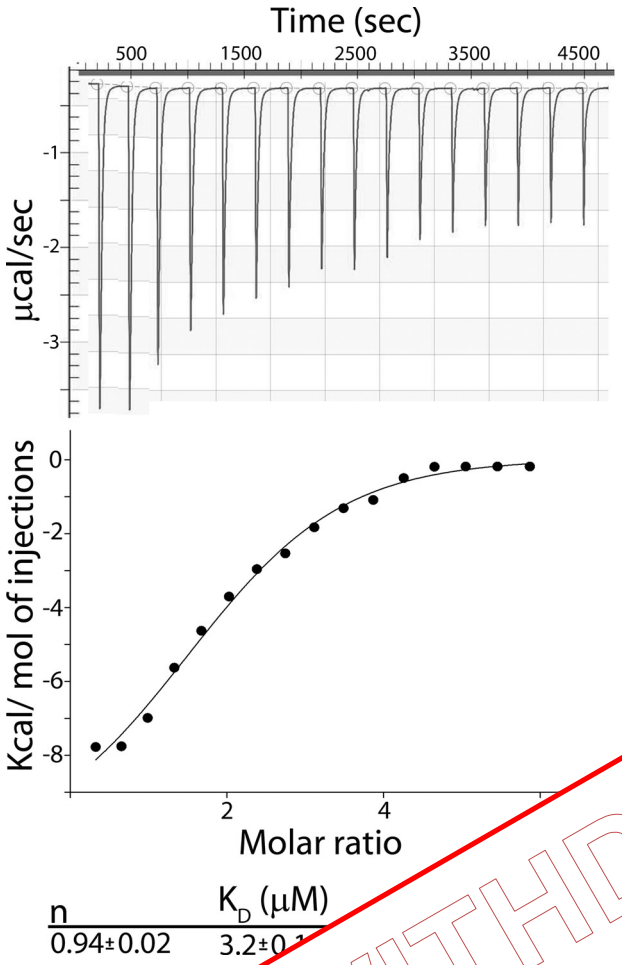

FIGURE 2. **Isothermal titrati… hexaose.** The *upper plot* show… the integrated heats of binding… out at 21 °C, by the addition of 7…

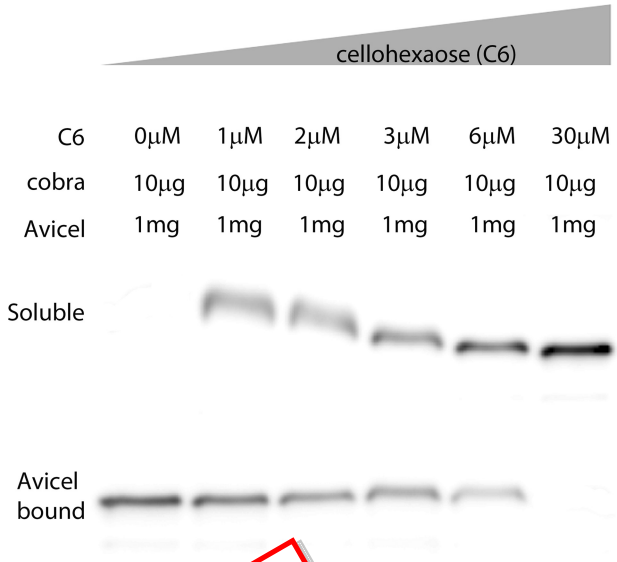

FIGURE 3. **COBRA competi… with crystalline cellulose (Avicel) and individual glucan… hexaose).** Pulldown assays of full-length COBRA and … with increasing concentrations of cellohexaose. … RA binds to Avicel. 1 µM Cello-hexaose w… fraction of COBRA from binding to Avi… esented a binding association … aose, a 10-fold increase over … ion bound to Avicel.

antibody, the washed pellet re… was bound to Avicel, and the soluble fraction … not bound to Avicel (Fig. 3). It is important to bea… mind that in this type of experiment, the individual glucan chains are soluble, whereas *in planta* they would be constrained by attachment to the cellulose synthase complex and/or hydrogen bonding to cellulose microfibrils. In the absence of cellohexaose, there is no detectable COBRA in the unbound portion (Fig. 3, 0 µM C6). As mentioned above, the COBRA K_D for cellohexaose was found to be 3.2 µM (Fig. 2), so we tested a range of cellohexaose concentrations below and above the K_D. When 1 µM cellohexaose was added to the reaction, a considerable fraction of COBRA remained in the soluble fraction, and this fraction increased when 2 µM cellohexaose was added to the reaction. With addition of 3 µM cellohexaose, more protein was detected in the soluble fraction compared with the Avicel-bound fraction, and with 30 µM cellohexaose, 10-fold above the K_D, COBRA was detected only in the soluble fraction and undetectable in the Avicel-bound fraction (Fig. 3). Along with the localization results, this finding raises the possibility that COBRA may act at the stage where individual β1–4-glucan chains have emerged from the complex and are being assembled into cellulose fibrils.

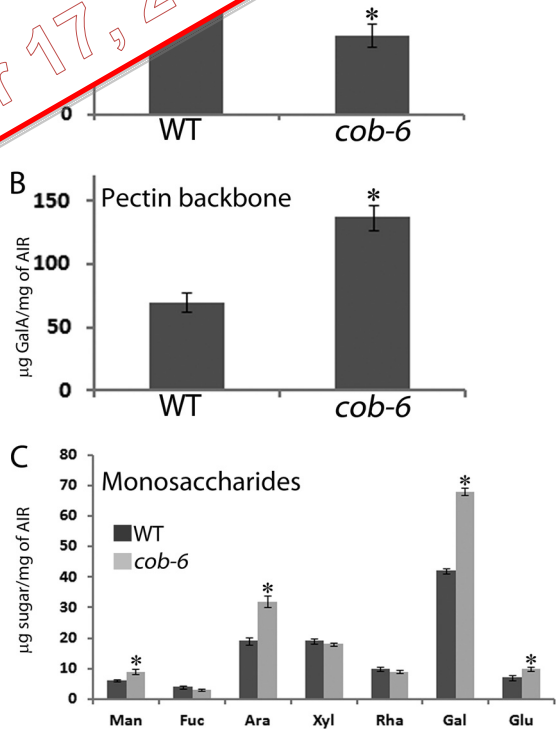

FIGURE 4. **Cell wall composition of WT and *cob-6*.** *A*, measurement of cellulose. *B*, analysis of galacturonic acid (GalA). *C*, monosaccharide analysis. In *A* and *B*, *asterisks* represent $p < 0.05$ by *t* test and in *C* the *asterisks* represent $p < 0.05$ by two-way analysis of variance coupled to Tukey test.

We characterized the effect of mutation in *COBRA* on the cell wall composition (Fig. 4) and structure (Figs. 5 and 6). *cob-6* has a reduction of 50% in the amount of cellulose (Fig. 4*A*), and

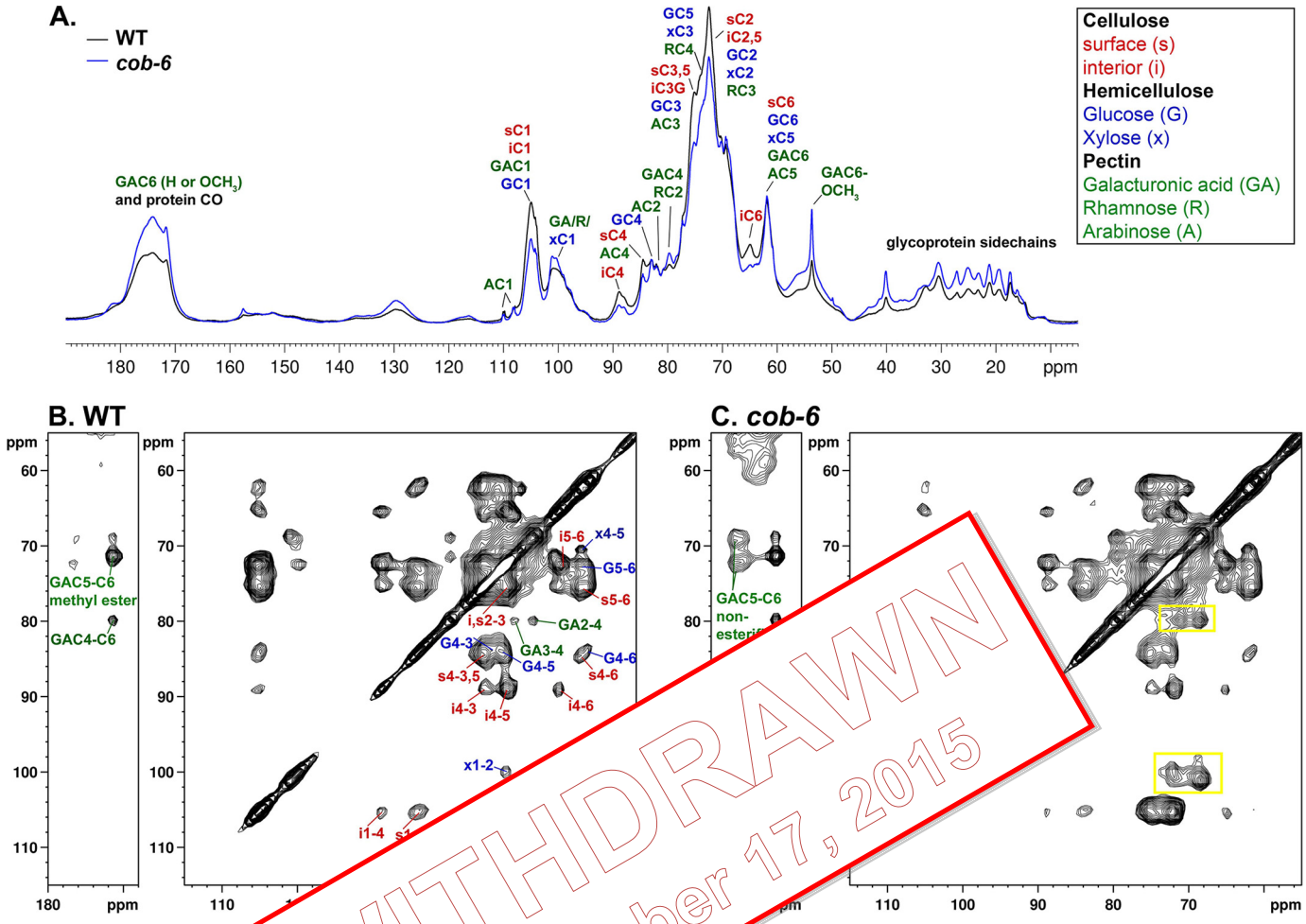

FIGURE 5. **One- and two-dir** ^{13}C direct polarization-MAS ssNMR spectra of WT and *cob-6* cell walls. *B* and *C*, ^{13}C-^{13}C chemical shi onal resonance mixing of WT (*B*) and *cob-6* (*C*). Assignments are indicated by color for cellulose (*red*), her *angles* indicate polysaccharides whose amounts changed in *cob-6* compared with the WT and relative to the

fewer overall glucan chains i (Fig. 5). It has been shown that the redu se in the *cobra* mutant is accompanied by overp n of starch, preventing osmotic stress by the excess of glucose that cannot be incorporated into the cell wall (36). Analysis of galacturonic acid (GalA) levels revealed a significant increase in the *cobra* mutant (Fig. 4*B*), and *Arabinose* (Ara) and galactose (Gal) levels also were increased (Fig. 4*C*). Galacturonic acid forms the backbone of the pectic polymers, and arabinose and galactose are abundant in the pectin side chains, implying a significant increase of the pectic fraction in the *cobra* mutant. To further characterize the cellulose fibrils that form in the *cobra* mutant, we used MAS ssNMR spectroscopy (Figs. 5 and 6).

Magic angle spinning solid-state NMR spectroscopy has already been proven to be a feasible technique to investigate the structure and intermolecular interactions of polysaccharides in intact plant cell walls (30, 37, 38). Previous ssNMR studies have yielded important structural information on primary *Arabidopsis* cell walls (39–41).

We used ssNMR to further analyze the molecular structure of the polysaccharides in WT and *cob-6* dark grown seedlings grown in liquid ½MS media with ^{13}C-labeled glucose (30) to obtain detailed information about crystalline cellulose structure. Spectra were measured quantitatively by ^{13}C direct polarization ssNMR using a long recycle delay (Fig. 5*A*). The one-dimensional ^{13}C-spectra show that the amount of cellulose in *cob-6* is considerably lower than in WT. Furthermore, the ratio between the intensity of the interior C4 peak (iC4) to surface C4 peak (sC4) in cellulose (40) was measured and indicates that *cob-6* has 16% lower crystallinity relative to WT (Table 4). In addition, we observed the peak at 88 ppm, which is indicative of a degree of crystallinity that is intermediate between the surface and interior cellulose (40).

When a short relaxation delay was utilized to increase the intensities of dynamic polysaccharides, the 88 ppm peak intensity was preferentially enhanced in *cob-6* relative to WT. We measured two-dimensional ^{13}C-^{13}C CP-dipolar-assisted rotational resonance spectra to detect through space contacts between carbons (Fig. 5, *B* and *C*). Qualitative inspection of the two-dimensional spectra shows that the relative intensities of hemicellulose and pectin cross-signals is significantly higher in *cob-6* compared with WT. We also observed that *cob-6* is not only rich in pectin, but the amount of non-esterified galacturonic acid is significantly higher than in WT. A comparison of the two-dimensional spectra revealed additional cross-peaks in the *cob-6* spectrum, which are absent in the WT spectrum even

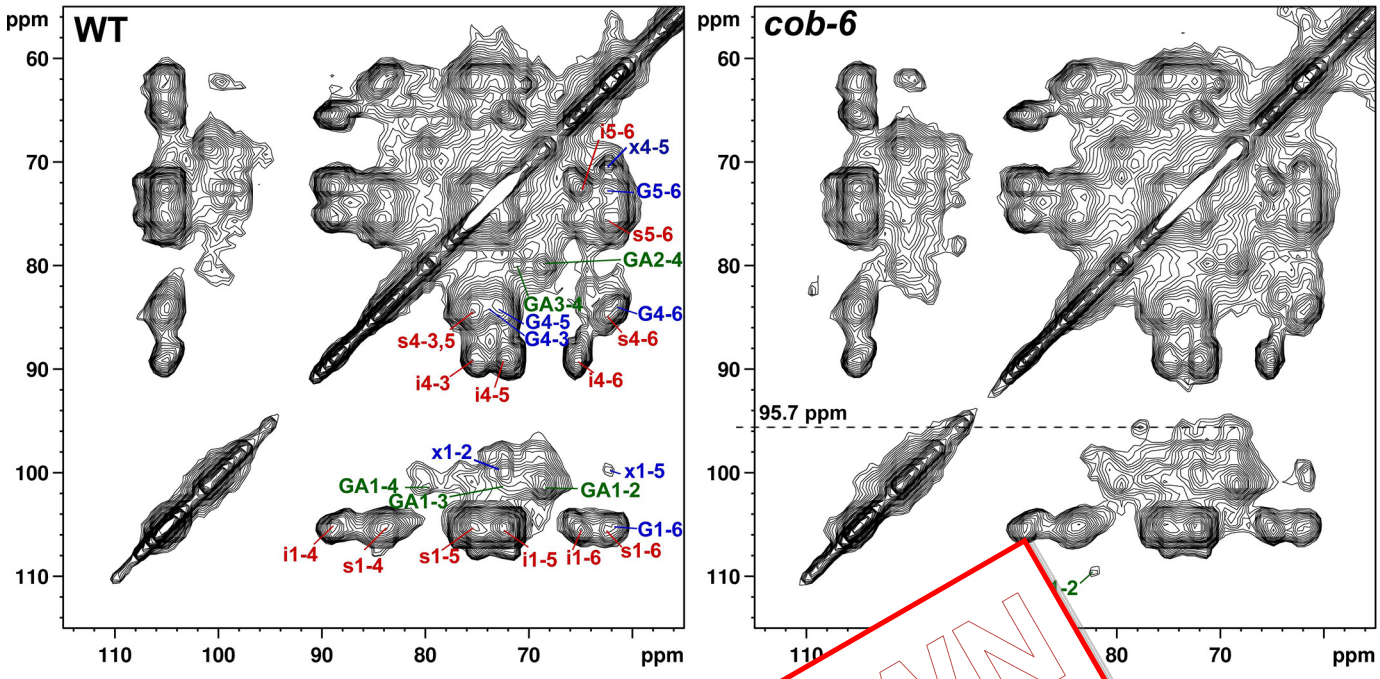

FIGURE 6. **^{13}C-^{13}C chemical shift correlation spectra of WT and *cob-6* acquired wi… resonance mixing time.** The spectra from Fig. 4 was plotted at lower contour levels, emphasizing the cross-sect… oss-section signals have been assigned to the β-glucose reducing end units, which can be detected when t… ly low.

TABLE 4

Relative intensities of interior and surface cellulose C4 ^{13}C-labeled DP-MAS spectra

Genotype	I(iC4) 88.5–91.5 ppm	I(sC4) 84 – 86 ppm
WT	36.4E9	54.5E…
cob-6	20.2E9	3…

at lower counter levels (… as Fig. 7). The apparent ppm, which is characteris… due to an effect of the devel- shift of a glucose monomer … as observed by Liu *et al.* (21). They cific chemical shifts we obser… may be released from the membrane in from a β-glucose reducing end… developmentally regulated hydrolysis of the higher concentration of short glu… cell imaging of the cellulose synthase complex in the …-6 mutant did not reveal any obvious defect in the rate of cellulose polymerization in the mutant once polymerization was initiated, nor any apparent difference from the wild type in the orientation of cellulose deposition. The disorganization of cellulose observed by electron microscopy (19) may not be due to *cobra per se*, but rather reflect an altered manner by which the defective microfibrils shift during expansion. There is also no apparent difference in the abundance of cellulose synthase complexes. Thus, we infer that the reduced amount of cellulose measured in the *cobra* mutants, as well as the increased number of cellulose-associated reducing ends evident by NMR, reflect an alteration in a process downstream of glucan polymerization.

DISCUSSION

COBRA was one of the first proteins suggested to be involved in cellulose formation (18) but its role has remained obscure. Previous immunoelectron microscopy studies suggested that COBRA was primarily located in the cell wall (19, 21), although the protein carries a motif that would be expected to lead to attachment of a GPI anchor. We found, by live-cell imaging, that COBRA was located in particles in the plasma membrane but did not observe any labeling in the cell wall. These particles are potentially the same as those containing CESAs, although because there are a fewer number of COBRA particles than CESA containing particles, we infer that cellulose synthase complexes would not always be associated with COBRA. Also, we observed a difference between the average velocity of movement of the COBRA-containing particles and the CESA-containing particles, suggesting that, if COBRA associates with cellulose synthase, it would be a slow-moving subset of CESA particles or a transient interaction such as initiation of micro-

The evidence that COBRA is in the plasma membrane (Fig. 1) and can bind cellulose and individual glucan chains (Figs. 2 and 3) leads us to hypothesize that COBRA functions after glucan polymerization at the step of cellulose formation in which individual chains emerge from the complex and are aligned to form cellulose fibrils (Fig. 7). Thus, we propose that COBRA is a kind of "polysaccharide chaperone" that facilitates cellulose crystallization. We hypothesize that, in the absence of COBRA, crystallization takes place with lower fidelity leading to the formation of partially "amorphous cellulose," which leads to the swollen cells that are characteristic of *cobra* mutants. The reduction in the amount of cellulose may be due to the defect in the ability to control turgor-induced cell expansion, or to deg-

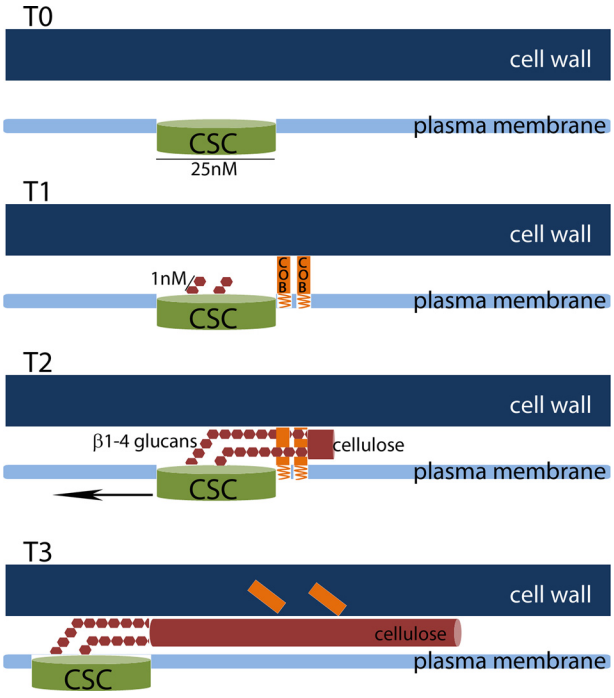

FIGURE 7. **Speculative model for the stages of cellulose formation.** *T0*, cellulose synthase complex (*CSC*) is targeted and integrated into the plasma membrane. *T1*, COBRA is recruited to the vicinity of the cellulose synth complex. Upon activation of the cellulose synthase complex, in β1–4-glucose chains emerge from the complex. *T2*, during the cellulose synthesis, the β1–4-glucose chains (in the model for simplicity) are bound by COBRA proteins, one gluca cule of COBRA protein. COBRA facilitates the int chains into a cellulose fibril. *T3*, if COBRA does lose microfibrils it would eventually be fo sized cellulose fibrils displace older fi

radation of amorphous KORRIGAN. The appare lose microfibrils inferred fr *cob-6* mutant is consistent with this ulate organization of COBRA, evident fro maging, presumably reflects accumulation of m RA proteins in close proximity. This organization is compatible with the idea that many COBRA molecules would be required in close proximity during cellulose formation because many glucan strands must be co-crystallized. In view of our observation that COBRA does not appear to be associated with the CESA complexes, we propose that COBRA acts transiently at the initiation of cellulose microfibrils to align the glucans as they emerge from the cellulose synthase complex, after which the process does not require COBRA participation. Because it is GPI-anchored, COBRA may help keep the growing cellulose microfibril at the plasma membrane during the initial stages of microfibril formation. If COBRA does not dissociate from the glucan chains, it could eventually be displaced into the cell wall by newly synthesized cellulose fibrils.

Cellulose-synthesizing bacteria do not have detectable homologs of *COBRA*. However, these bacteria do not incorporate cellulose into cell wall structures and the fibrils are smaller than those from higher plants and not coated with hemicellulose. Most importantly perhaps, plant cellulose microfibrils are tightly appressed between the site of synthesis in the plasma membrane and the adjacent cell wall, whereas bacterial microfibrils are not. This may create a tight bend in the glucan chains as they emerge from the plant cellulose synthase, which may impose a need for the proposed COBRA activity that the bacterial process lacks. Alternatively, the presence in plant cell walls of hemicellulose polysaccharides, which hydrogen-bond to cellulose, may impose a need for shielding of the newly synthesized glucans during the process of crystallization to form cellulose microfibrils.

Acknowledgments—We thank Trevor Yeats for helpful advice and comments on the manuscript, and Ana B. Ibáñez, Abigail A. Landers, and Erin Imsand for advice and excellent technical assistance.

REFERENCES

1. Somerville, C., Bauer, S., Brininstool, G., Facette, M., Hamann, T., Milne, J., Osborne, E., Paredez, A., Persson, S., Raab, T., Vorwerk, S., and Youngs, H. (2004) Toward a systems a roach to understanding plant cell walls. *Science* **306,** 2206–2211
2. Bashline, L., Lei, L. 2014) Cell wall, cytoskeleton, and cell expansion in **7,** 586–600
3. McFarla on, S. (2014) The cell biology of cell **65,** 69–94
4. Delmer, D. P. (2002) Cellulose tes. *Plant Cell Physiol.* **43,**
rdt, D. W. (2006) Visualization nctional association with microtu-
R., and Gu, Y. (2012) Cellulose synthase inter- 1) links microtubules and cellulose synthase com- tl. Acad. Sci. U.S.A.* **109,** 185–190
C., and Persson, S. (2012) Co-expression of cell-wall related s: new tools and insights. *Front. Plant Sci.* **3,** 83
Nicol, F., His, I., Jauneau, A., Vernhettes, S., Canut, H., and Höfte, H. (1998) A plasma membrane-bound putative endo-1,4-β-D-glucanase is required for normal wall assembly and cell elongation in *Arabidopsis*. *EMBO J.* **17,** 5563–5576
9. Zuo, J., Niu, Q. W., Nishizawa, N., Wu, Y., Kost, B., and Chua, N. H. (2000) KORRIGAN, an *Arabidopsis* endo-1,4-β-glucanase, localizes to the cell plate by polarized targeting and is essential for cytokinesis. *Plant Cell* **12,** 1137–1152
10. His, I., Driouich, A., Nicol, F., Jauneau, A., and Höfte, H. (2001) Altered pectin composition in primary cell walls of korrigan, a dwarf mutant of *Arabidopsis* deficient in a membrane-bound endo-1,4-β-glucanase. *Planta* **212,** 348–358
11. Szyjanowicz, P. M., McKinnon, I., Taylor, N. G., Gardiner, J., Jarvis, M. C., and Turner, S. R. (2004) The irregular xylem 2 mutant is an allele of korrigan that affects the secondary cell wall of *Arabidopsis thaliana*. *Plant J.* **37,** 730–740
12. Lei, L., Zhang, T., Strasser, R., Lee, C. M., Gonneau, M., Mach, L., Vernhettes, S., Kim, S. H., Cosgrove, J., Li, S., and Gu, Y. (2014) The jiaoyao1 mutant is an allele of korrigan1 that abolishes endoglucanase activity and affects the organization of both cellulose microfibrils and microtubules in *Arabidopsis*. *Plant Cell* **26,** 2601–2616
13. Vain, T., Crowell, E. F., Timpano, H., Biot, E., Desprez, T., Mansoori, N., Trindade, L. M., Pagant, S., Robert, S., Höfte, H., Gonneau, M., and Vernhettes, S. (2014) The cellulase KORRIGAN is part of the cellulose synthase complex. *Plant Physiol.* **165,** 1521–1532
14. Persson, S., Wei, H., Milne, J., Page, G. P., and Somerville, C. R. (2005) Identification of genes required for cellulose synthesis by regression analysis of public microarray data sets. *Proc. Natl. Acad. Sci. U.S.A.* **102,** 8633–8638
15. Sánchez-Rodríguez, C., Bauer, S., Hématy, K., Saxe, F., Ibáñez, A. B., Vodermaier, V., Konlechner, C., Sampathkumar, A., Rüggeberg, M., Aich-

inger, E., Neumetzler, L., Burgert, I., Somerville, C., Hauser, M. T., and Persson, S. (2012) Chitinase-like1/pom-pom1 and its homolog CTL2 are glucan-interacting proteins important for cellulose biosynthesis in *Arabidopsis*. *Plant Cell* **24,** 589–607
16. Benfey, P. N., Linstead, P. J., Roberts, K., Schiefelbein, J. W., Hauser, M. T., and Aeschbacher, R. A. (1993) Root development in *Arabidopsis*: four mutants with dramatically altered root morphogenesis. *Development* **119,** 57–70
17. Brady, S. M., Song, S., Dhugga, K. S., Rafalski, J. A., and Benfey, P. N. (2007) Combining expression and comparative evolutionary analysis: the COBRA gene family. *Plant Physiol.* **143,** 172–187
18. Schindelman, G., Morikami, A., Jung, J., Baskin, T. I., Carpita, N. C., Derbyshire, P., McCann, M. C., and Benfey, P. N. (2001) COBRA encodes a putative GPI-anchored protein, which is polarly localized and necessary for oriented cell expansion in Arabidopsis. *Gene Dev.* **15,** 1115–1127
19. Roudier, F., Fernandez, A. G., Fujita, M., Himmelspach, R., Borner, G. H., Schindelman, G., Song, S., Baskin, T. I., Dupree, P., Wasteneys, G. O., and Benfey, P. N. (2005) COBRA, an *Arabidopsis* extracellular glycosylphosphatidylinositol-anchored protein, specifically controls highly anisotropic expansion through its involvement in cellulose microfibril orientation. *Plant Cell* **17,** 1749–1763
20. Eisenhaber, B., Wildpaner, M., Schultz, C. J., Borner, G. H., Dupree, P., and Eisenhaber, F. (2003) Glycosylphosphatidylinositol lipid anchoring of plant proteins. Sensitive prediction from sequence- and genome-wide studies for arabidopsis and rice. *Plant Physiol.* **133,** 1691–1701
21. Liu, L., Shang-Guan, K., Zhang, B., Liu, X., Yan, M., Zhang, L., Shi, Y., Zhang, M., Qian, Q., Li, J., and Zhou, Y. (2013) Brittle Culm1, a COBRA-like protein, functions in cellulose assembly through binding cellulose microfibrils. *Plos Genet.* **9,** e1003704
22. Sato, K., Ito, S., Fujii, T., Suzuki, R., Takenouchi, S., Nakaba, S., F… Sano, Y., Kajita, S., Kitano, H., and Katayama, Y. (2010) The… binding module (CBM)-like sequence is crucial for ri… tion in proper assembly of secondary cell wall… *Behav.* **5,** 1433–1436
23. Estévez, J. M., and Somerville, C. (200… imaging of synthetic peptides e… *Techniques* **41,** 569–570, 5…
24. DeBolt, S., Gutierrez, R., … motile cellulose synthase s… regions at the plasma memb… …ng 2,6-dichlorobenzonitrile treat…
25. Todd, M. J., and Gomez, J. (200… …ed using calorimetry: a general assay for e… *…al. Biochem.* **296,** 179–187
26. Walter, S., and Schrempf, H. (2003) C… …rization, membrane anchoring, and cellulose-binding characteristics of AbpS, a receptor-like *Streptomyces* protein. *J. Biol. Chem.* **278,** 26639–26647
27. Bauer, S., and Ibáñez, A. B. (2014) Rapid determination of cellulose. *Biotechnol. Bioeng.* **111,** 2355–2357
28. Morcombe, C. R., and Zilm, K. W. (2003) Chemical shift referencing in MAS solid state NMR. *J. Magn. Reson.* **162,** 479–486
29. Fung, B. M., Khitrin, A. K., and Ermolaev, K. (2000) An improved broadband decoupling sequence for liquid crystals and solids. *J. Magn. Reson.* **142,** 97–101
30. Dick-Pérez, M., Zhang, Y., Hayes, J., Salazar, A., Zabotina, O. A., and Hong, M. (2011) Structure and interactions of plant cell-wall polysaccharides by two- and three-dimensional magic-angle-spinning solid-state NMR. *Biochemistry* **50,** 989–1000
31. Takegoshi, K., Nakamura, S., and Terao, T. (2001) C-13-H-1 dipolar-assisted rotational resonance in magic-angle spinning NMR. *Chem. Phys. Lett.* **344,** 631–637
32. Brabham, C., and Debolt, S. (2012) Chemical genetics to examine cellulose biosynthesis. *Front. Plant Sci.* **3,** 309
33. Scheible, W. R., Eshed, R., Richmond, T., Delmer, D., and Somerville, C. (2001) Modifications of cellulose synthase confer resistance to isoxaben and thiazolidinone herbicides in Arabidopsis Ixr1 mutants. *Proc. Natl. Acad. Sci. U.S.A.* **98,** 10079–10084
34. Lis, H., and Sharon, N. (1998) Lectins: carbohydrate-specific proteins that mediate cellular recognition. *Chem. Rev.* **98,** 637–674
35. Boraston, A. B., Bolam, D. N… …bert, H. J., and Davies, G. J. (2004) Carbohydrate-binding m… …-tuning polysaccharide recognition. *Biochem. J.* **382,** 7…
36. Dai, X., You… …, Q., and Wu, C. (2011) OsBC1L4 encod… …fects cellulose synthesis in rice. *Pl…*
… …MR of cellulose. *Curr. Opin.*
… …(2012) Whole plant cell wall … NMR. *Nat. Protoc.* **7,** 1579–1589
… …al, A., Zabotina, O. A., and Hong, M. …id-state NMR studies of the structure and …saccharides in uniformly ^{13}C-labeled *Arabidopsis* … *Magn. Reson. Chem.* **50,** 539–550
… …L., Corbin, K., Wang, T., Gutierrez, R., Bertolo, A. L., Petti, C., …s, D. M., Estevez, J. M., Bonetta, D., Urbanowicz, B. R., Ehrhardt, … W., Somerville, C. R., Rose, J. K., Hong, M., and Debolt, S. (2012) Cellulose microfibril crystallinity is reduced by mutating C-terminal transmembrane region residues CESA1(A903V) and CESA3(T942I) of cellulose synthase. *Proc. Natl. Acad. Sci. U.S.A.* **109,** 4098–4103
41. Wang, T., Zabotina, O., and Hong, M. (2012) Pectin-cellulose interactions in the *Arabidopsis* primary cell wall from two-dimensional magic-angle-spinning solid-state nuclear magnetic resonance. *Biochemistry* **51,** 9846–9856
42. Carroll, A., Mansoori, N., Li, S., Lei, L., Vernhettes, S., Visser, R. G., Somerville, C., Gu, Y., and Trindade, L. M. (2012) Complexes with mixed primary and secondary cellulose synthases are functional in *Arabidopsis* plants. *Plant Physiol.* **160,** 726–737

The *Arabidopsis* COBRA Protein Facilitates Cellulose Crystallization at the Plasma Membrane

Nadav Sorek, Hagit Sorek, Aleksandra Kijac, Heidi J. Szemenyei, Stefan Bauer, Kian Hématy, David E. Wemmer and Chris R. Somerville

J. Biol. Chem. 2014, 289:34911-34920.
doi: 10.1074/jbc.M114.607192 originally published online October 20, 2014